can be seen in the middle to upper stratosphere in the Northern Hemisphere. This effect may be responsible for the decrease in stratospheric temperature at high latitudes (Fig. 30) where a positive anomaly for total heating was found (Fig. 35). On the other hand, the increase in meridional eddy transport of moisture in the troposphere (Fig. 43) may be attributable to the overall increase in water vapor in the atmosphere.

Changes in precipitation (Fig. 44) and its components (Figs. 45 and 46) and in river runoff (Fig. 47) occur at smaller spatial scales than those in temperature. In general, precipitation increases in regions where much precipitation was computed in the C run. It was also found that the interannual variability of precipitation at low latitudes was much affected by the model ENSO and interdecadal variations shown in the previous section. Increase in precipitation at high latitudes did not contribute to an increase in snow depth except for the polar region (Figs. 48 and 49) because of the warming effect.

A shift of air mass due to the warming contrast between the oceans and continents can be seen in the change in sea level pressure (Figure 50). A distinct positive anomaly in sea level pressure was found in the subtropical North Pacific Ocean. Soil moisture (Fig. 51) decreased over almost all the continents at middle latitudes, suggesting that the change in soil moisture enhanced the ocean-land warming contrast.

Finally, changes in clouds (Fig. 52) and components of heat fluxes at the top (net downward shortwave radiation, Fig. 53; net outgoing longwave radiation, Fig. 54), and at the surface of the atmosphere (sensible heat, Fig. 55; latent heat, Fig. 56; net downward shortwave radiation, Fig. 57; net upward longwave radiation, Fig. 58) are shown. In relation to the change in sea ice in the Okhotsk Sea, a large decrease in sensible heat flux can be seen over the Okhotsk Sea (Fig. 55).

6 Concluding remarks

A coupled atmosphere-ocean general circulation model has been developed. The model is characterized by two aspects; a relatively high resolution of the oceanic component at low latitudes to simulate El Niño phenomena and an elaborate sea ice model to simulate seasonal variations of sea ice coverage and thickness. The transient response of the climate to gradual increase in atmospheric

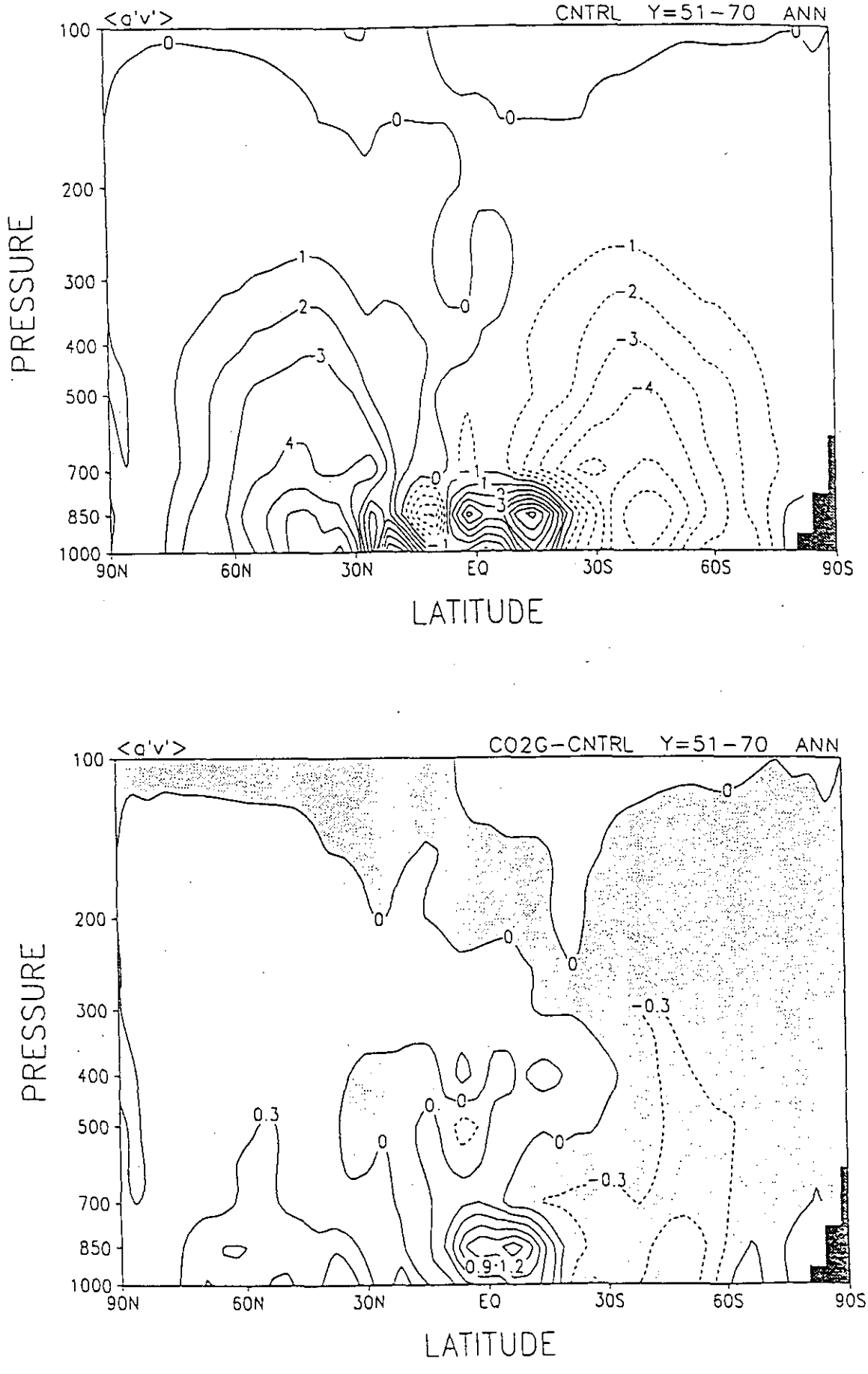

Fig. 43 As in Fig. 32 but for meridional eddy moisture transport. Contour intervals are 1 g/Kg·m/s (upper panel) and 0.3 g/Kg·m/s (lower panel).

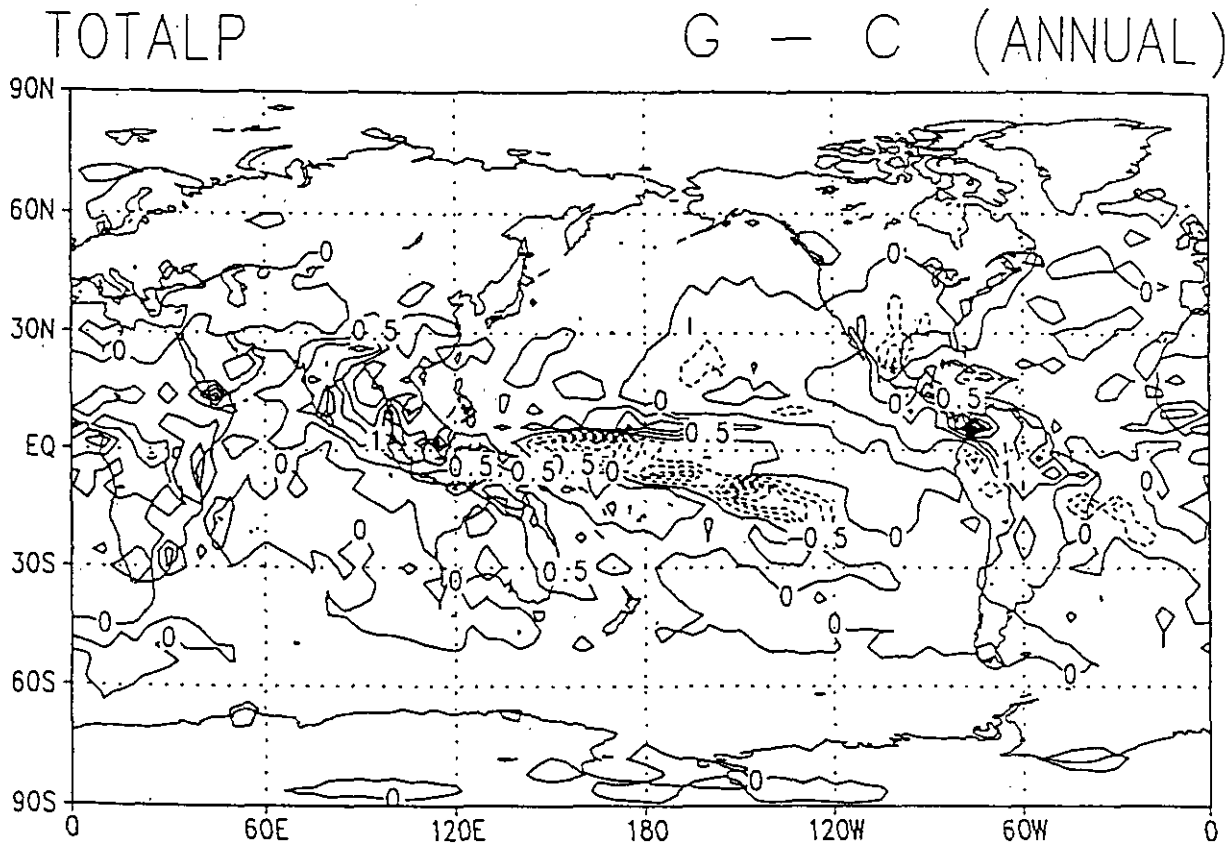

Fig. 44 Change, G - C, in annual-mean precipitation (mean of years 51-70). Contour interval is 0.5 mm/day.

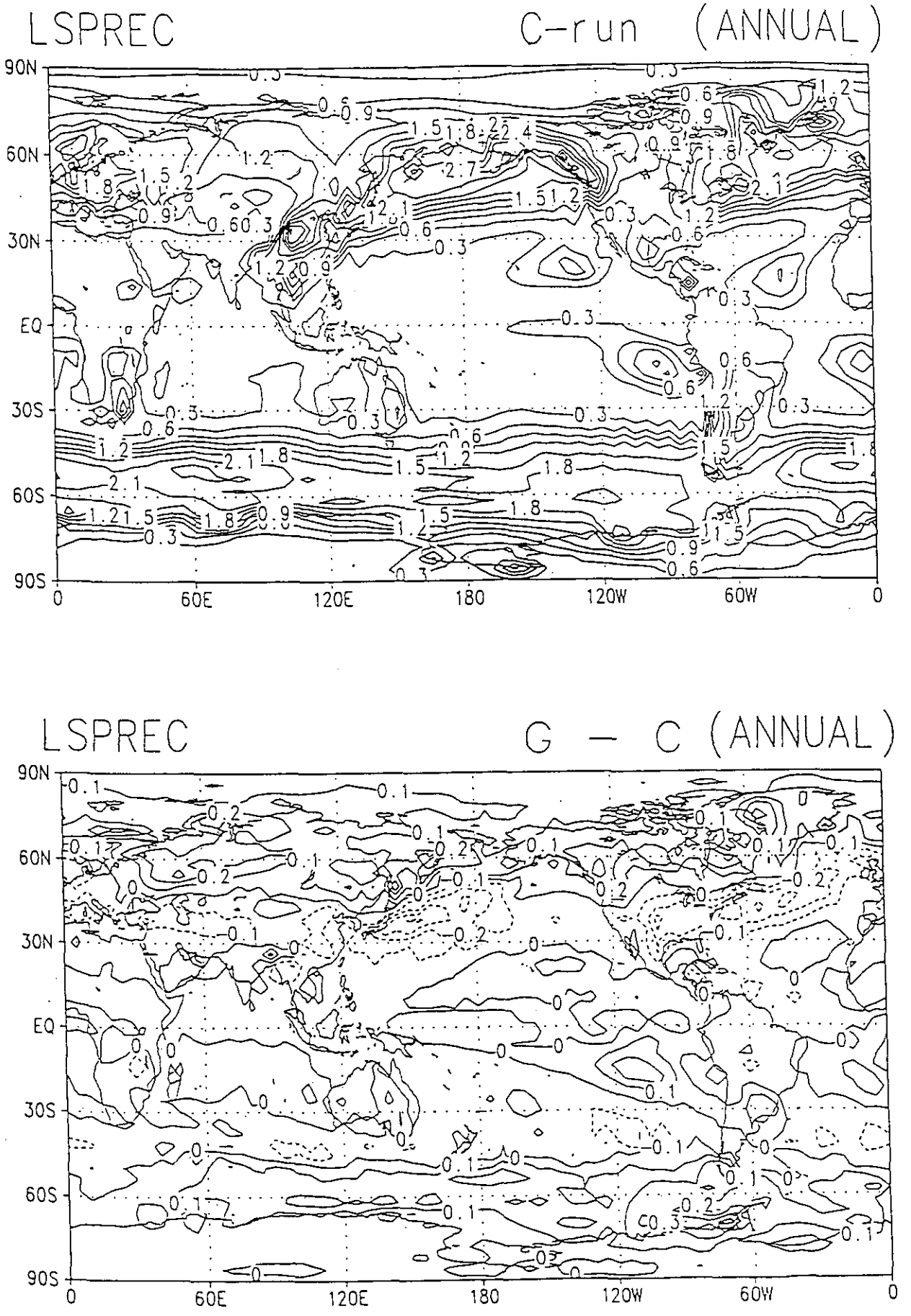

Fig. 45 Annual-mean precipitation due to large scale condensation for the C run (upper panel) and its change, G - C, (lower panel). Both are averaged over years 51-70. Contour intervals are 0.3 mm/day (upper panel) and 0.1 mm/day (lower panel).

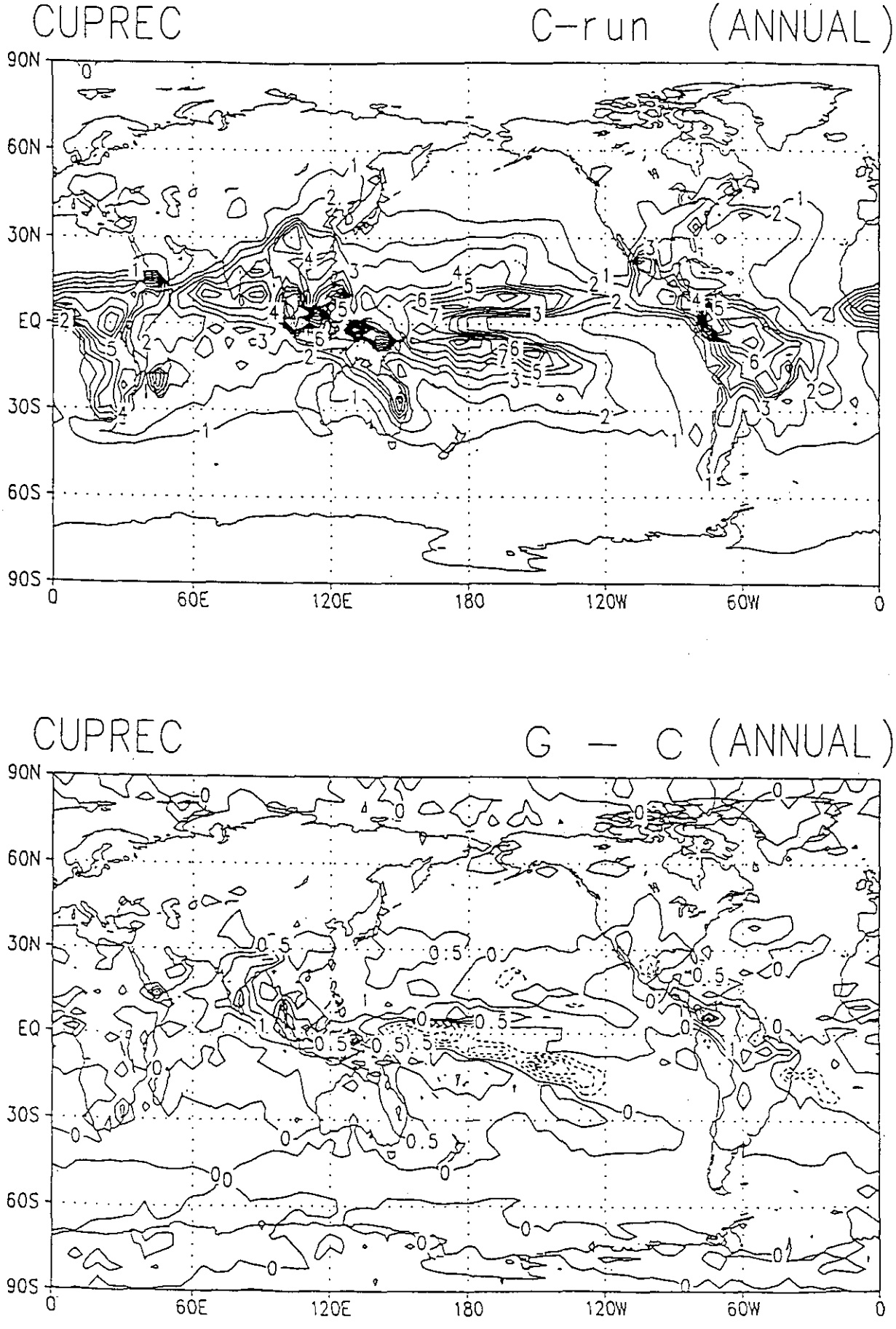

Fig. 46 As in Fig. 45 but for precipitation due to cumulus convection. Contour intervals are 1 mm/day (upper panel) and 0.5 mm/day (lower panel).

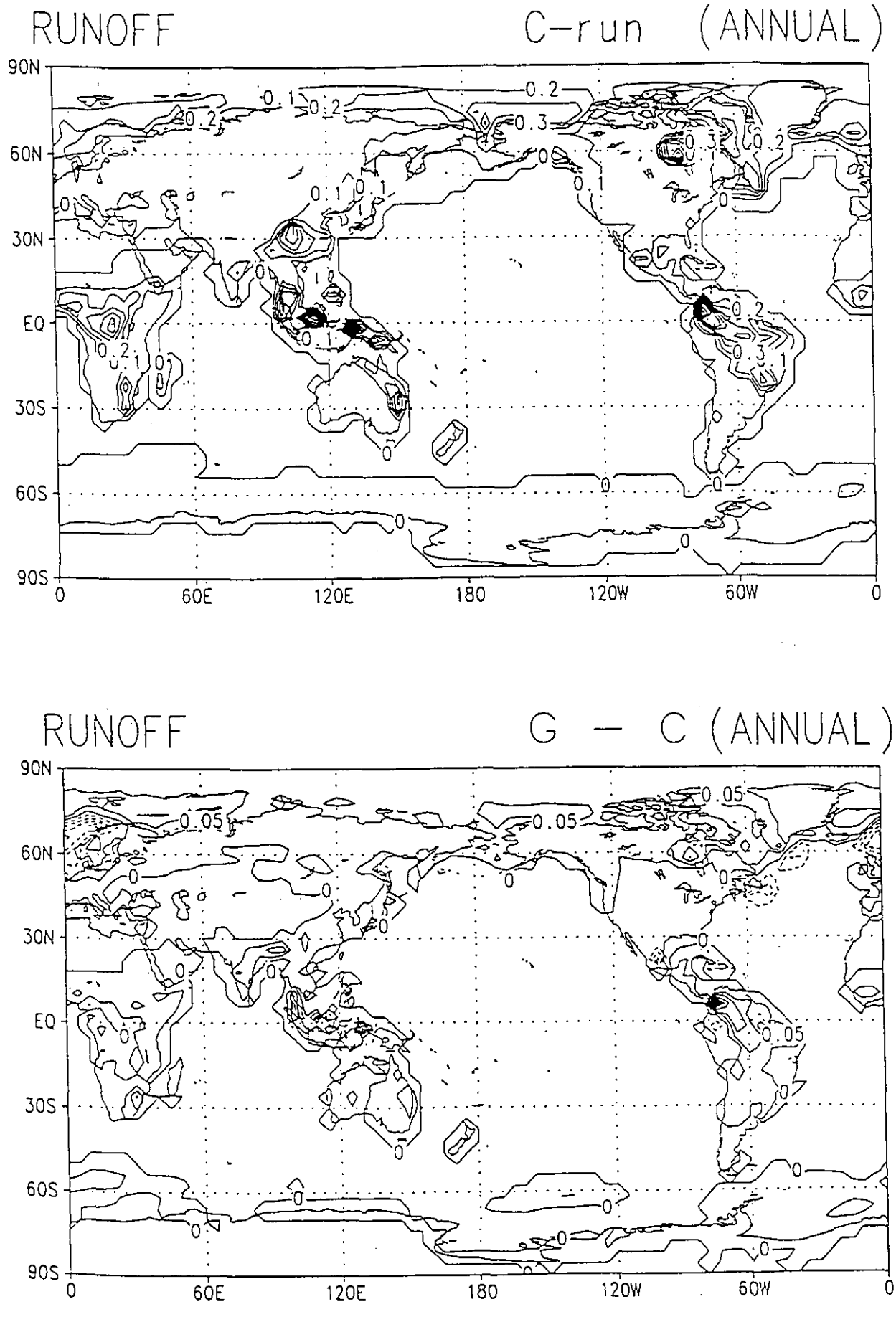

Fig. 47 As in Fig. 45 but for river runoff. Contour intervals are 0.1 mm/day (upper panel) and 0.05 mm/day (lower panel).

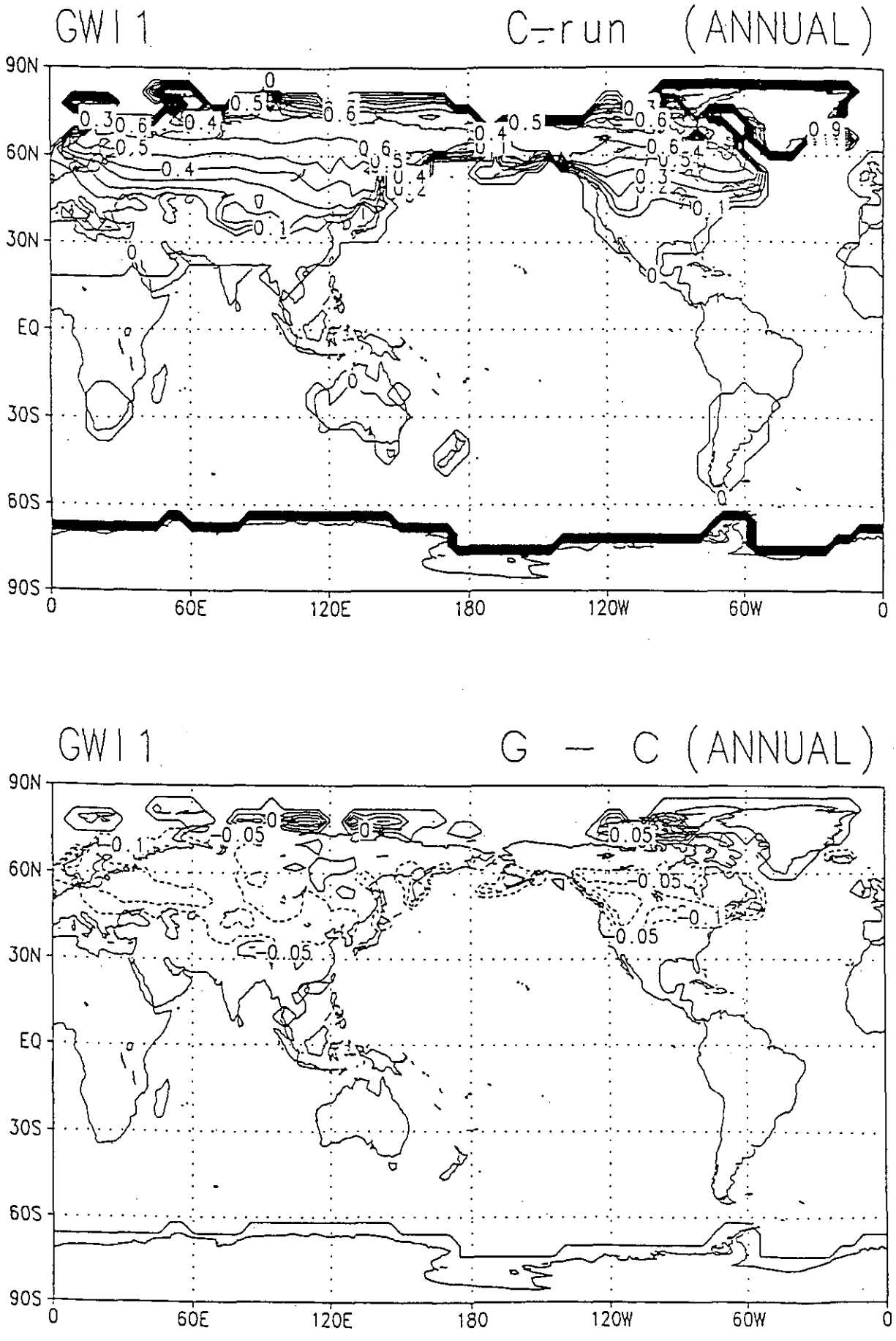

Fig. 48 As in Fig. 45 but for frozen soil moisture of the surface layer. Contour intervals are 0.1 (upper panel) and 0.05 (lower panel).

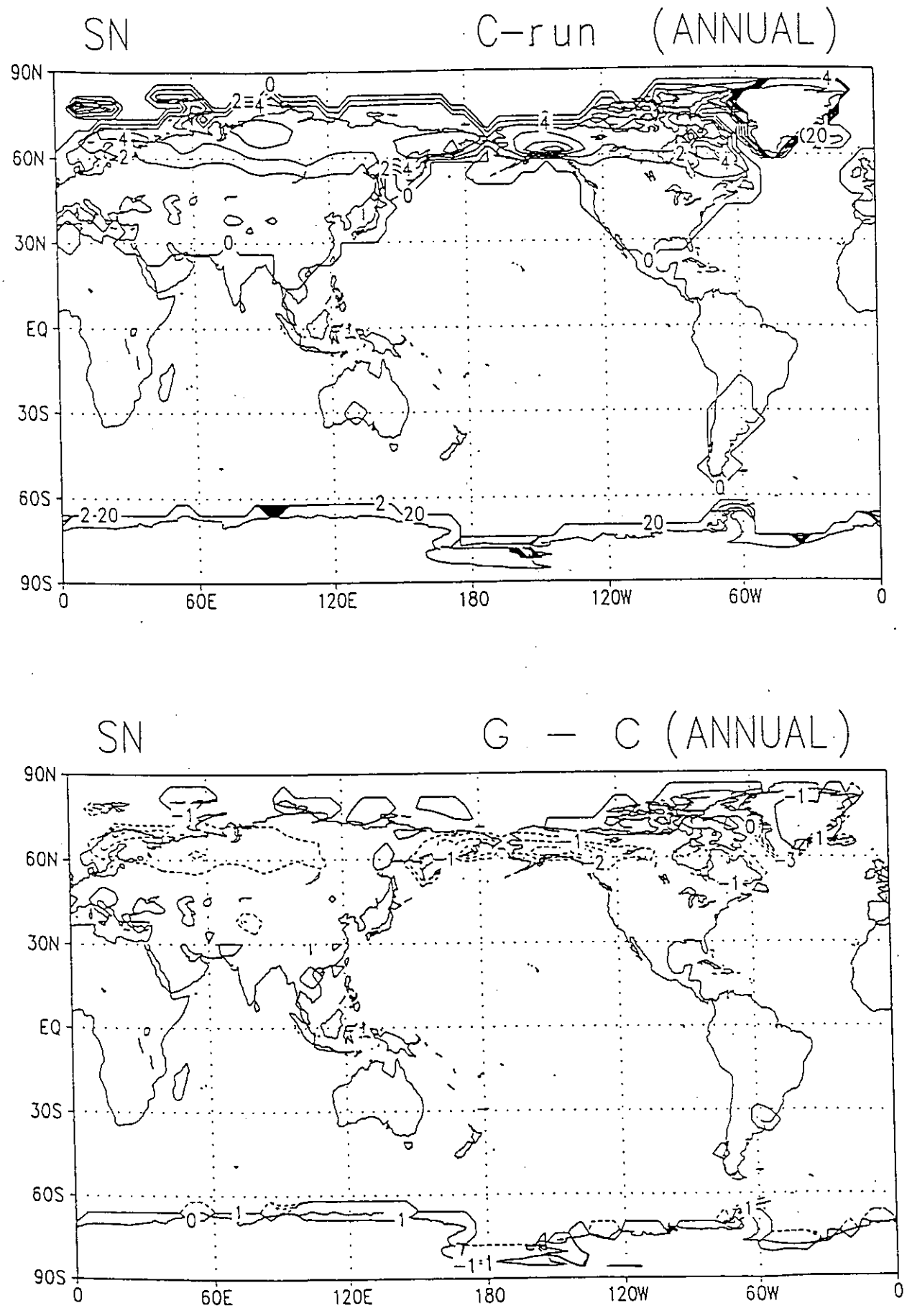

Fig. 49 As in Fig. 45 but for snow mass. Contour intervals are 2 cm (upper panel) and 1 cm (lower panel).

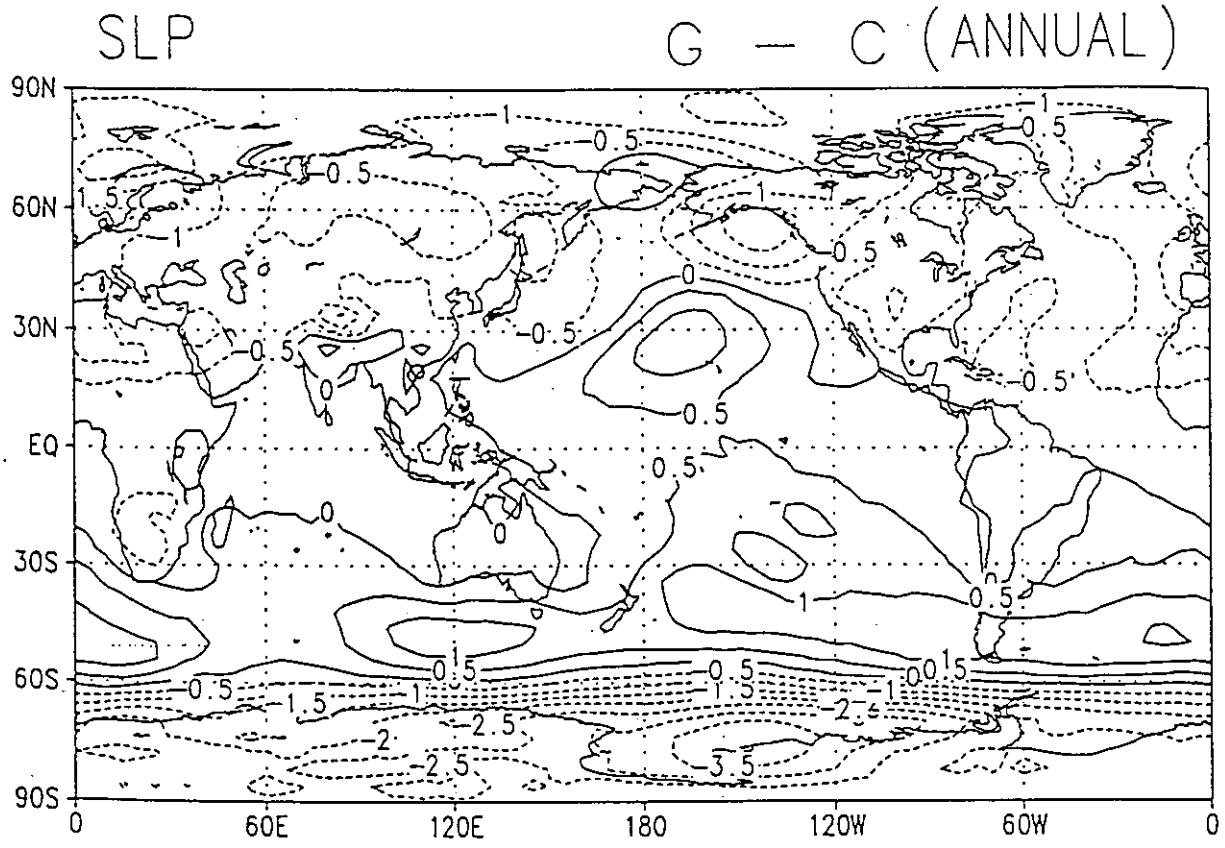

Fig. 50 As in Fig. 44 but for sea level pressure. Contour intervals is 0.5 hPa.

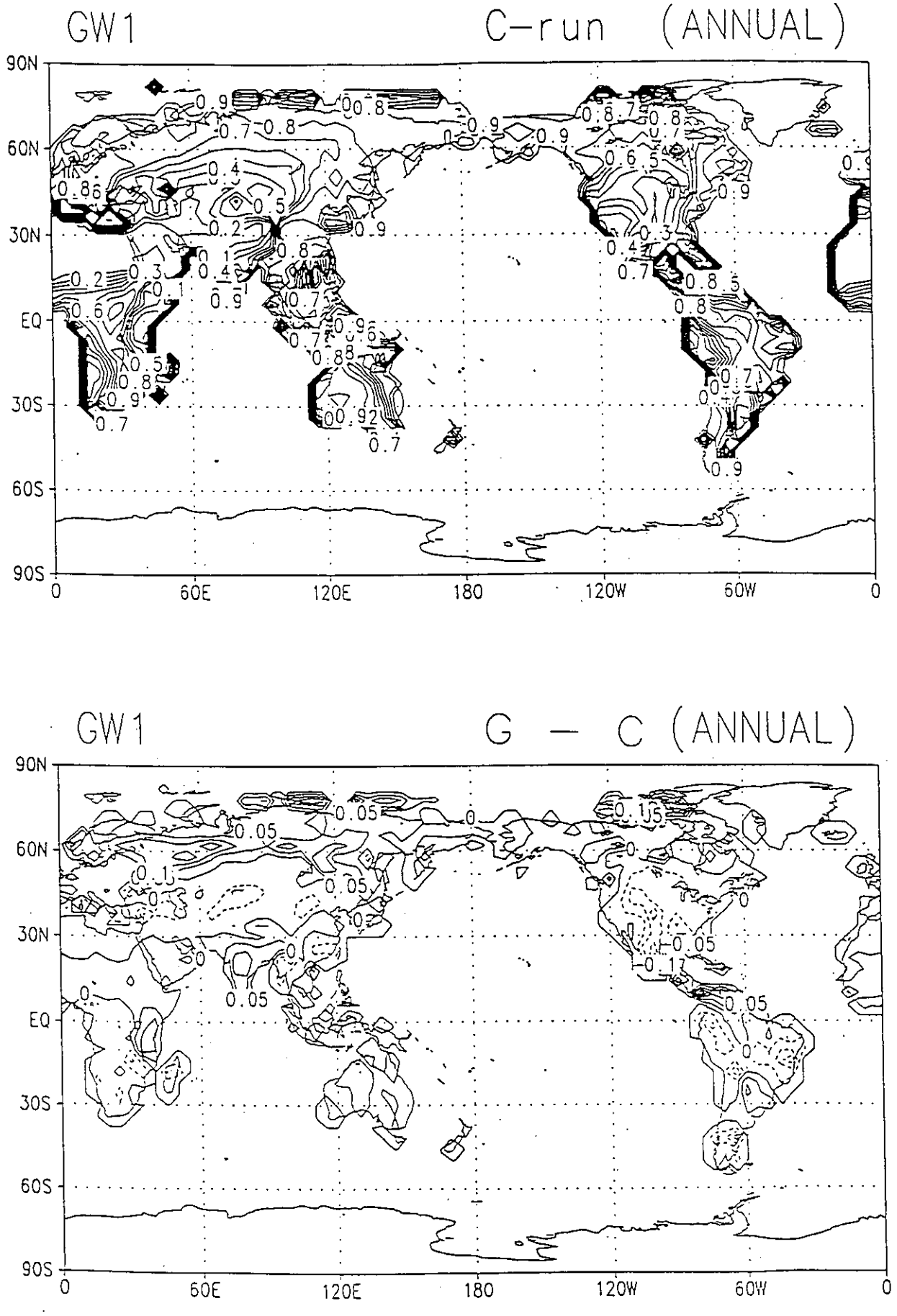

Fig. 51 As in Fig. 45 but for soil moisture of the surface layer. Contour intervals are 0.1 (upper panel) and 0.05 (lower panel).

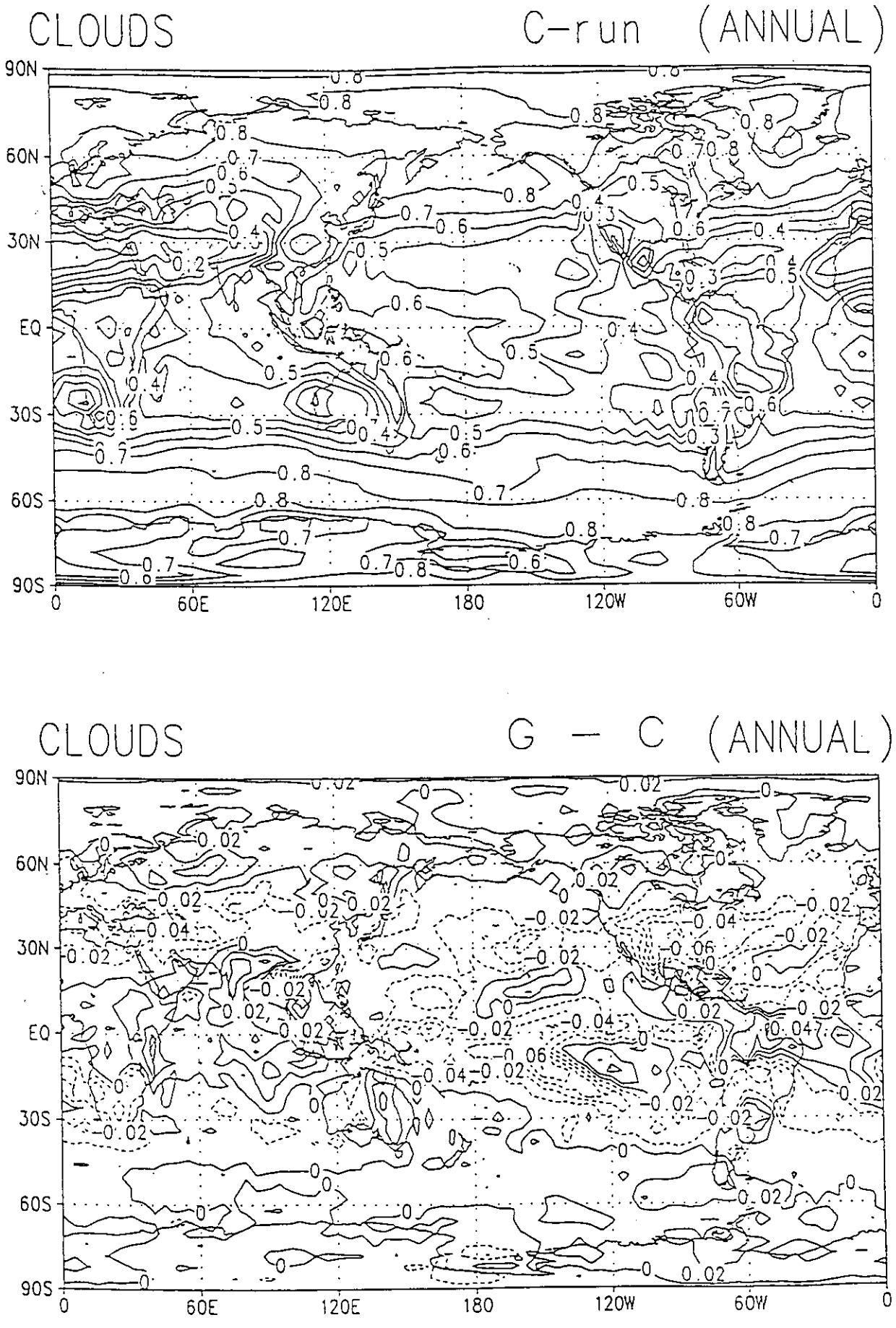

Fig. 52 As in Fig. 45 but for cloudiness. Contour intervals are 10 % (upper panel) and 1 % (lower panel).

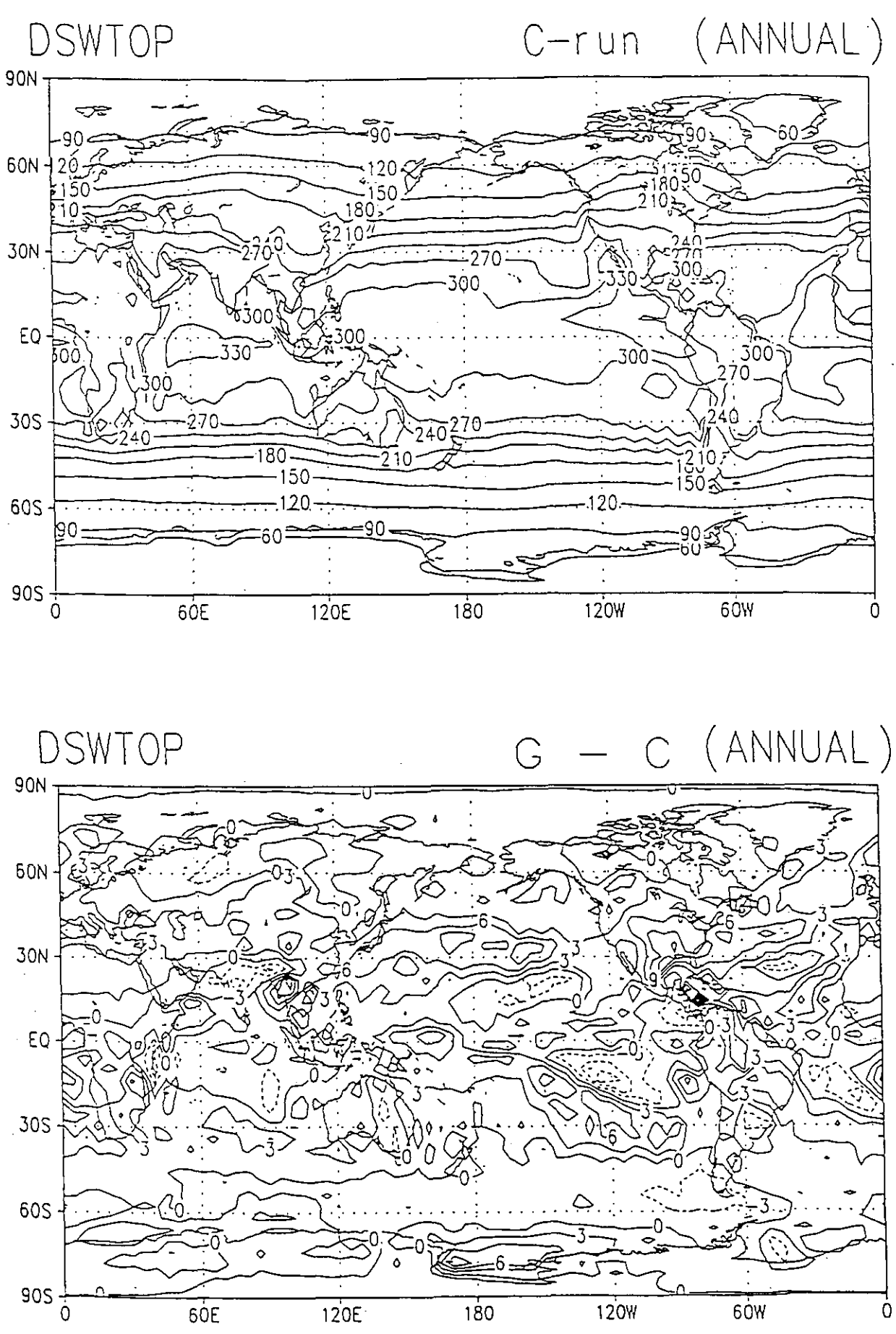

Fig. 53 As in Fig. 45 but for downward shortwave radiation at the top of the atmosphere. Contour intervals are 30 W/m^2 (upper panel) and 3 W/m^2 (lower panel).

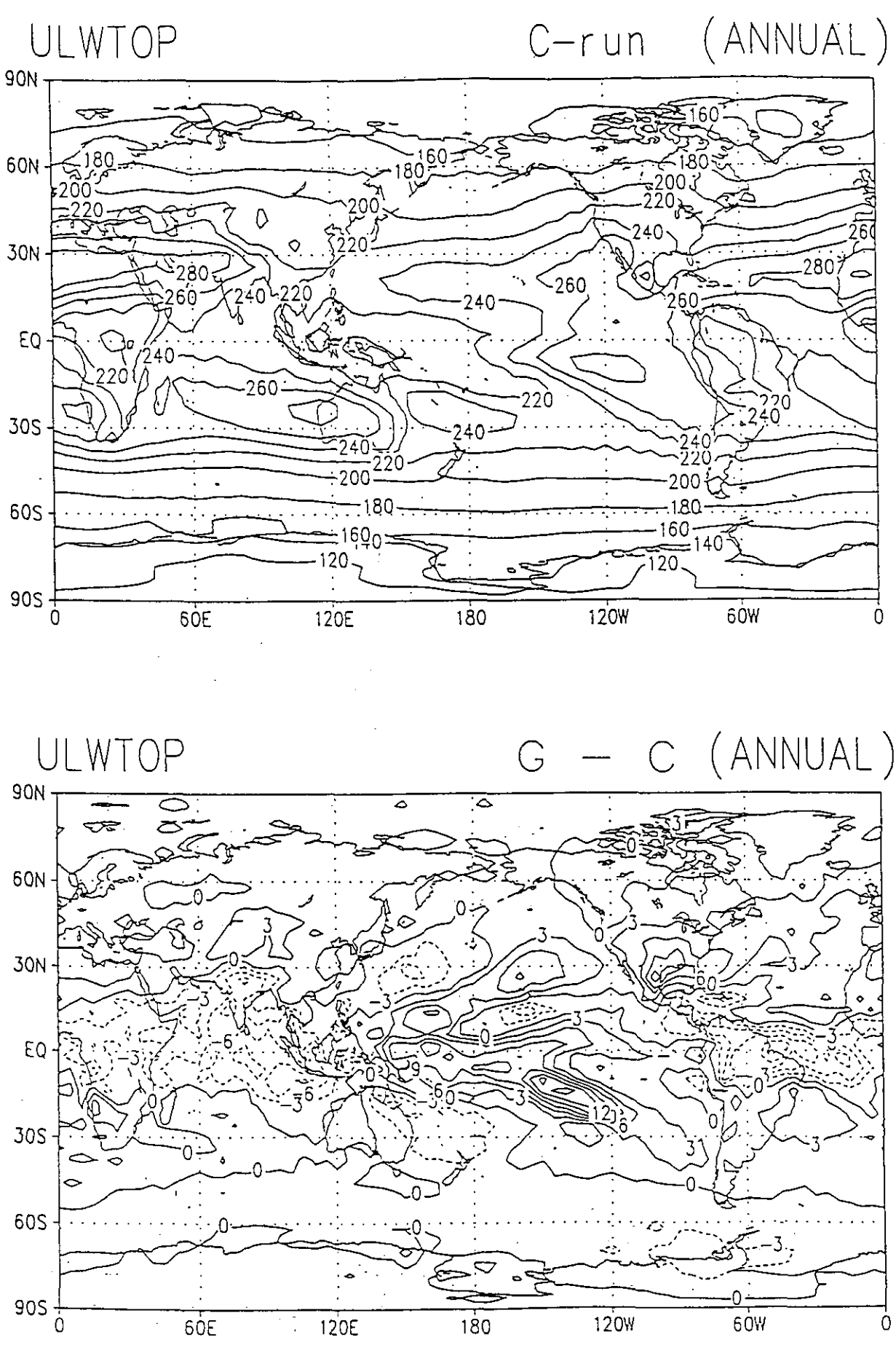

Fig. 54 As in Fig. 45 but for outgoing longwave radiation at the top of the atmosphere. Contour intervals are 20 W/m^2 (upper panel) and 3 W/m^2 (lower panel).

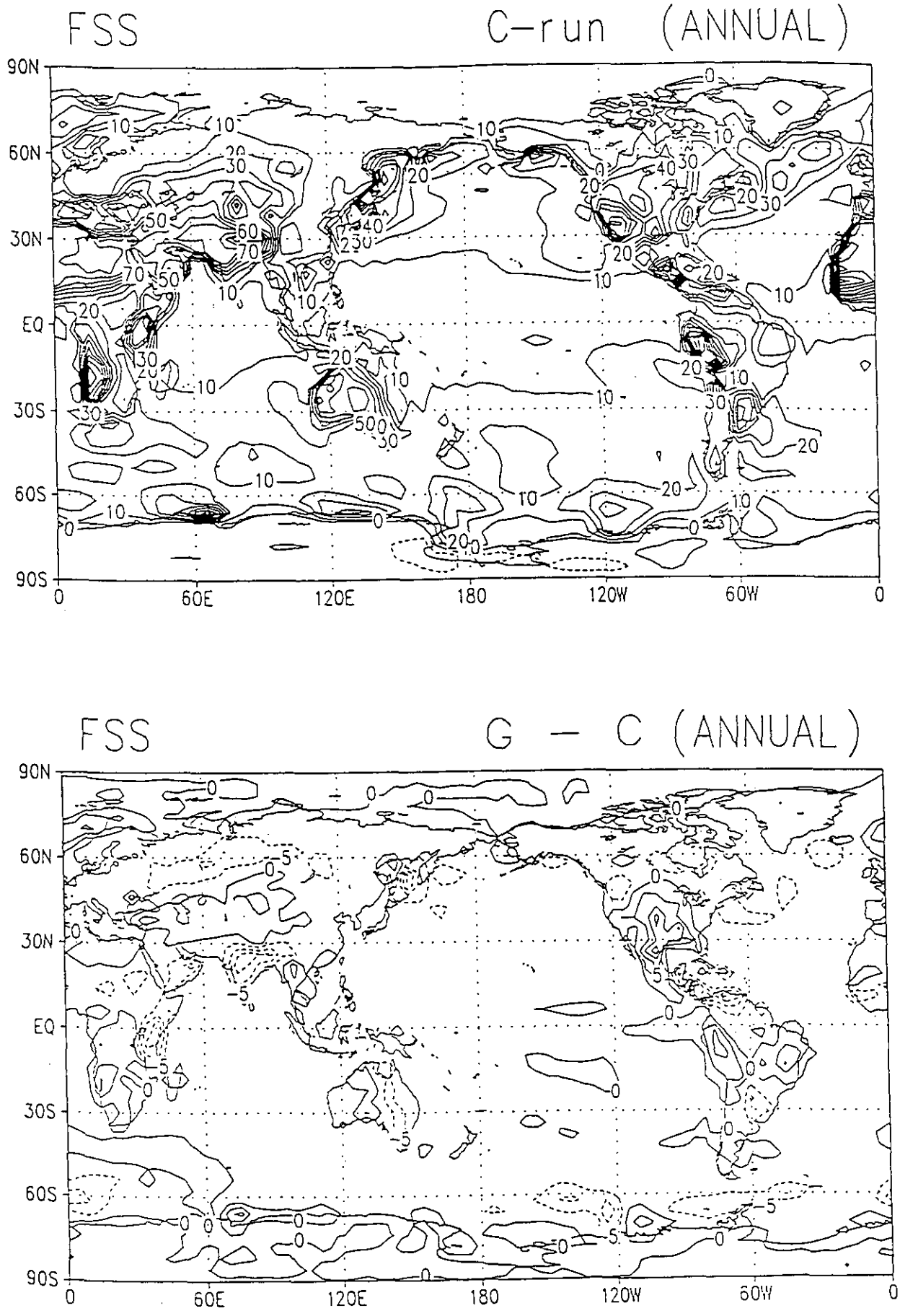

Fig. 55 As in Fig. 45 but for sensible heat flux at the surface. Contour intervals are 10 W/m^2 (upper panel) and 5 W/m^2 (lower panel).

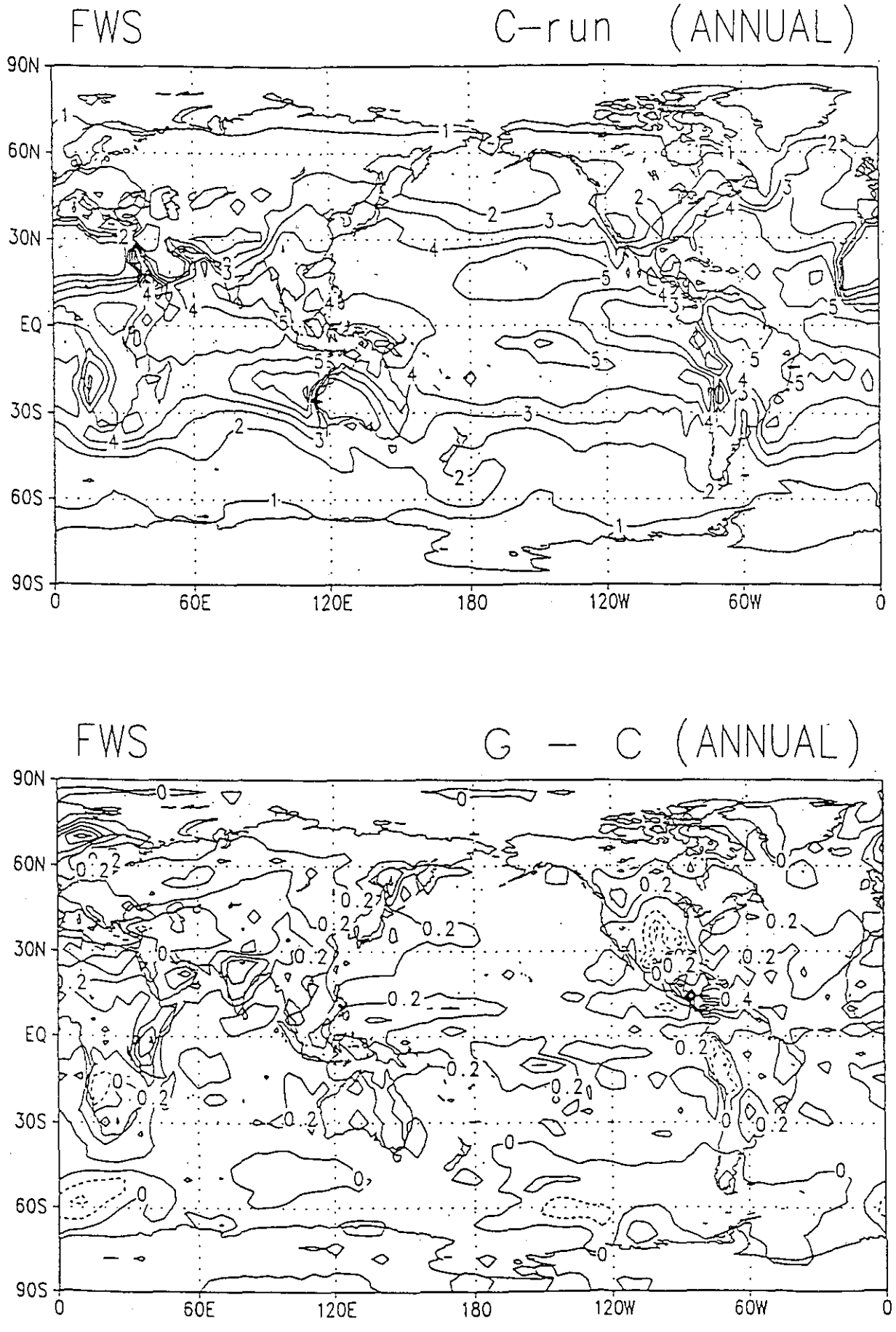

Fig. 56 As in Fig. 45 but for evaporation (latent heat flux) at the surface. Contour intervals are 1 mm/day (29.1 W/m^2) (upper panel) and 0.2 mm/day (lower panel).

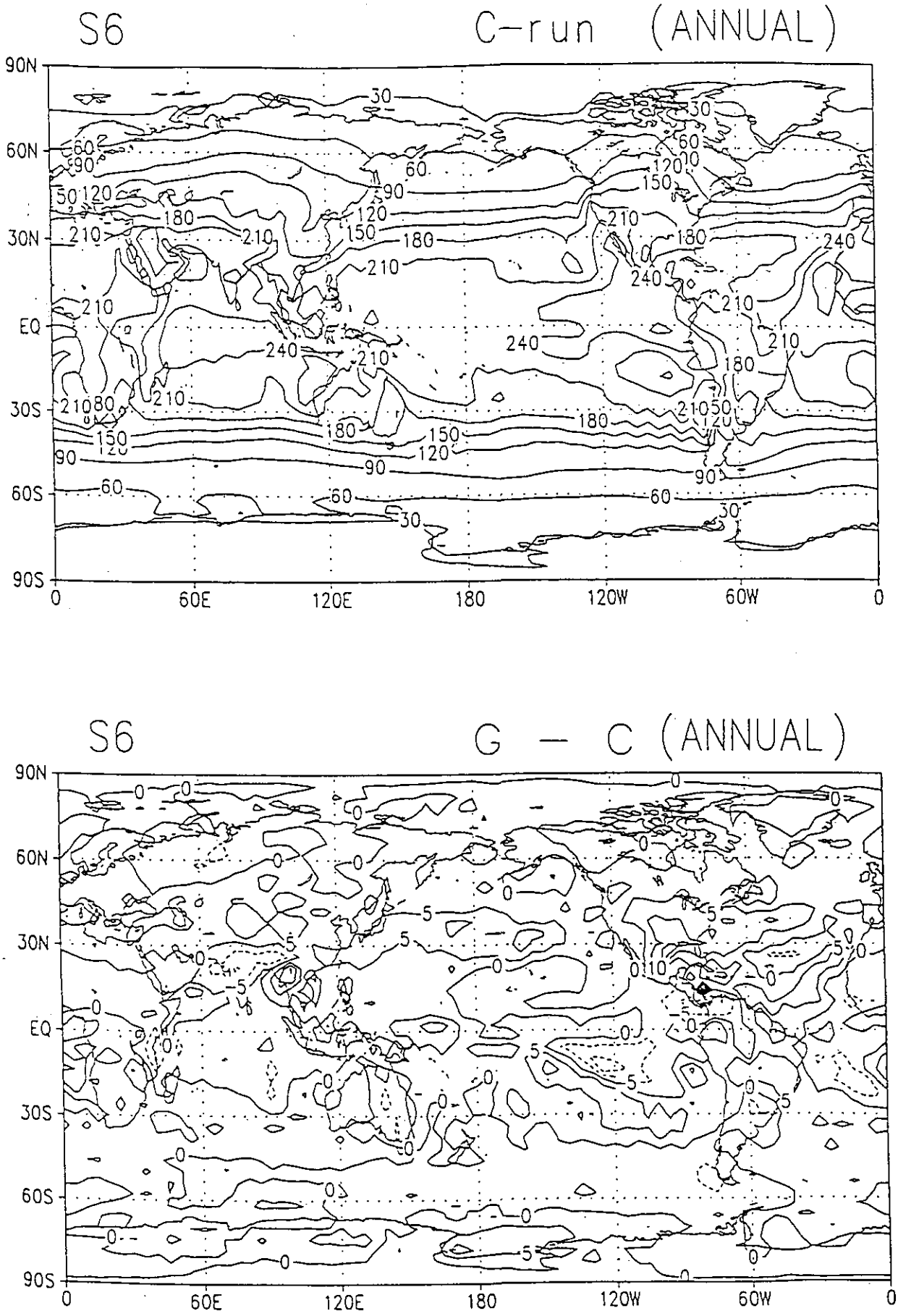

Fig. 57 As in Fig. 45 but for net shortwave radiation at the surface. Contour intervals are 30 W/m^2 (upper panel) and 5 W/m^2 (lower panel).

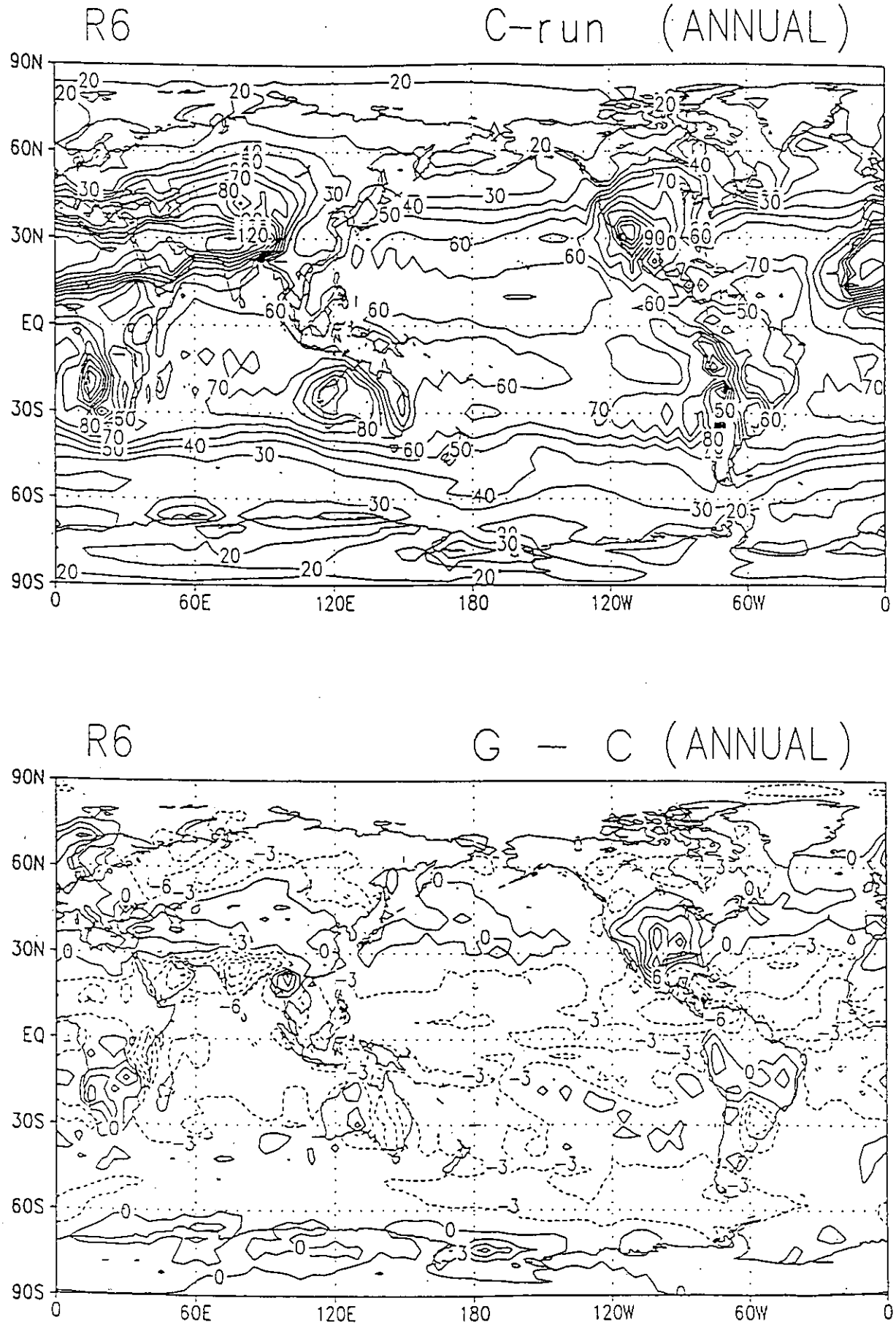

Fig. 58 As in Fig. 45 but for net longwave radiation at the surface. Contour intervals are 10 W/m^2 (upper panel) and 3 W/m^2 (lower panel).